Keywords: shipping, decarbonization, ammonia; NO_x, N_2O, emission control, GHG

Emission Control Concepts for large two-stroke ammonia engines

Georgia Voniati, Athanasios Dimaratos, Grigorios Koltsakis, Leonidas Ntziachristos

Laboratory of Applied Thermodynamics, Department of Mechanical Engineering, Aristotle University of Thessaloniki, 54124, Thessaloniki, Greece

https://doi.org/10.18453/rosdok_id00004637

Abstract

Decarbonizing the maritime sector to meet the ambitious IMO targets requires the integration of various technologies. Among the alternative fuels, ammonia (NH_3) is a promising candidate; however, its combustion generates NO_x, NH_3, and N_2O, a potent greenhouse gas (GHG). The current study explores emissions control strategies for NH_3-fueled marine engines, employing both conventional and advanced catalytic technologies in simulated NH_3 engine exhaust to eliminate the unwanted N-species from the combustion process. Small-scale experiments are conducted on a synthetic gas bench (SGB) using three catalytic samples: two SCR technologies (vanadium-based (V-SCR) and iron-based (Fe-SCR)), and a platinum-based NH_3 oxidation catalytic (Pt-AOC). These experiments provide reaction kinetics information which are then integrated into physico-chemical models. The V-SCR reaction scheme employed commonly used reactions, whereas the Fe-SCR required specific modifications to its chemical reaction scheme. The models are then used to examine two scenarios concerning the relative engine-out concentrations of NO_x, NH_3 and N_2O: (1) low NO_x with high NH_3 and N_2O, and (2) high NO_x with lower NH_3 and N_2O levels. Simulation results indicate that NO_x could be optimized to meet the IMO limits with minimum NH_3 slip in both cases. However, high levels of NH_3 in the exhaust gas can result to significantly increased N_2O production in the exhaust aftertreatment system. In the meantime, N_2O decomposition using a cobalt-based catalyst is being examined, though the potential effects of NO_x, NH_3 and SO_2 remain to be determined.

1. Introduction

International maritime shipping plays a crucial role in the global economy and trade. Nevertheless, vessel emissions have a significant impact both on the environment and the human health. In particular, the maritime sector is responsible for almost 3% of the global Greenhouse Gas (GHG) emissions, which is expected to further increase until 2050 [1]. Apart from GHG, the maritime sector is also a source of air pollutants, such as Nitrogen Oxides (NO_x), Sulfur Oxides (SO_x) and Particulate Matter (PM) emissions [2]. In efforts to mitigate global warming and environmental impact of shipping, the International Maritime Organization (IMO) has implemented more stringent regulations on ships' emissions, aiming to at least 70% reduction in GHG by 2040, and ultimately to net-zero GHG emissions around 2050 [3]. In parallel, NO_x emissions must adhere to Tier III standards (3.4 g/kWh for vessels powered by low-speed two-stroke engines) within Emission Control Areas (ECAs), and Tier II standards (14.4 g/kWh for vessels powered by low-speed two-stroke engines) globally. Regarding SO_x emissions, the IMO has implemented a global sulfur cap, setting a maximum limit of 0.50% fuel sulfur content that decreases to 0.10% within Sulfur Emission Control Areas (SECAs) [4].

In pursuit of this goal, the introduction of alternative fuels such as liquified natural gas (LNG), methanol, ethanol, liquid petroleum gas (LPG), ammonia and hydrogen can significantly reduce emissions and minimize environmental and health risks. Among the alternative fuels, ammonia (NH_3) is one of the most promising solutions for fueling marine engines as it is carbon-free, it is easily stored in liquid form, and can be produced utilizing renewable energy sources such as wind, solar, or hydroelectric power [5]. However, the poor combustion properties of NH_3 (high autoignition temperature, low flame speed, low flammability) preclude a stable combustion with pure ammonia. Consequently, a pilot-fuel with higher cetane number (i.e., Diesel) is used to initiate the combustion of ammonia [6,7]. In addition to the poor combustion properties, it is known that ammonia combustion produces Nitrous Oxide (N_2O), unburnt NH_3 and NO_x emissions [5]. The former is one of the strongest GHG, with Global Warming Potential (GWP) over 100-year period equal to almost 300 [8]. NO_x and NH_3 (from fuel combustion and the Exhaust Aftertreatment System (EATS) respectively), are commonly targeted emissions species. Conversely, N_2O has always been treated as an unwanted product of the EATS rather as an engine emission to be targeted by a catalytic device. Therefore, the EATS of NH_3 fueled engines needs to adapt in order to simultaneously control all unwanted N-species.

The application of a Selective Catalytic Reduction (SCR) system (vanadium-based usually in marine applications) is commonly employed to reduce NO_x emissions by utilizing NH_3 or urea as the reducing agent [9]. In the case of ammonia combustion, NO_x can undergo direct reaction with the unburnt NH_3, or NH_3 can be directly injected upstream of the SCR to ensure adequate reductant availability. Ammonia slip can be minimized with an ammonia slip catalyst (ASC), however oxidation of NH_3 can promote NO_x and N_2O formation. Advanced SCR formulations are studied towards N_2O abatement. Iron-based catalysts (Fe-SCR) can be advantageous due to their ability to simultaneously reduce NO_x and N_2O by NH_3 [10,11]. It would be highly desirable to convert N_2O via catalytic thermal decomposition without the need of a reducing agent. Cobalt-based catalysts have been reported to promote such thermal N_2O decomposition [12-16], albeit only at rather high temperatures.

Based on the above, it is evident that the catalytic technologies must be developed and adopted to simultaneously reduce the unwanted N-species of NH_3 engine exhaust. However, NH_3 engines, particularly large two-stroke ones, used in the maritime sector are not yet commercially available. Consequently, the exact exhaust gas conditions for designing an emission control system are not

precisely known. Even if the exhaust gas characteristics of NH_3 engines were available from measurements, designing an emission control system through trial and error would be prohibitive due to the enormous testing costs on large two-stroke marine engines. Therefore, it is imperative to develop accurate and predictive models of the aftertreatment system that are applicable under a wide range of conditions to ensure the coverage of all possible scenarios. The development of such models is essentially the main target of the present work which is conducted within the EU-funded ENGIMMONIA project.

Exhaust aftertreatment models rely on kinetic mechanisms and rate expressions that describe the intrinsic chemical properties of the active materials. In this study, experiments are performed to derive the respective kinetic information for three catalytic formulations of interest and introduce them in integrated physico-chemical models of the transient transport and the reaction processes in monolithic catalytic reactors. The models are then used to study possible scenarios concerning the relative engine-out concentrations of NO_x, NH_3 and N_2O. The base scenario assumes an NH_3 to NO_x ratio of less than 1 (ANR<1) with low N_2O emissions, so additional NH_3 is injected upstream of the SCR, while the alternative scenario assumes low NO_x with high NH_3 (ANR>1) and higher N_2O emissions. The activity of the commonly used vanadium-based SCR (V-SCR) is compared to the Fe-SCR based technology. In the case of high NH_3 concentration in the exhaust, a dual-layer ASC is integrated to the aftertreatment system to handle the NH_3 slip. Particular emphasis is given to the formation/reduction of N_2O and the equivalent CO_2-emissions accounting for CO_2 emissions from pilot fuel as well.

2. Experimental and Modeling methods

2.1. Small-scale catalyst testing

The study of the catalyst chemistry is supported by measurements conducted on a Synthetic Gas Bench (SGB) setup (Figure 1). The flow rate and composition are regulated using the programmable mass flow controllers (MFCs). Moisture is introduced into the mixture via a pre-heated H_2O feed to avoid flue gas condensation. Subsequently, the mixture is heated to the desired temperature using a pre-heater system before traversing through the catalyst sample. The concentrations of the species at the outlet of the catalyst are quantified using an FTIR gas analyzer (AVL Sesam i60 FT SII).

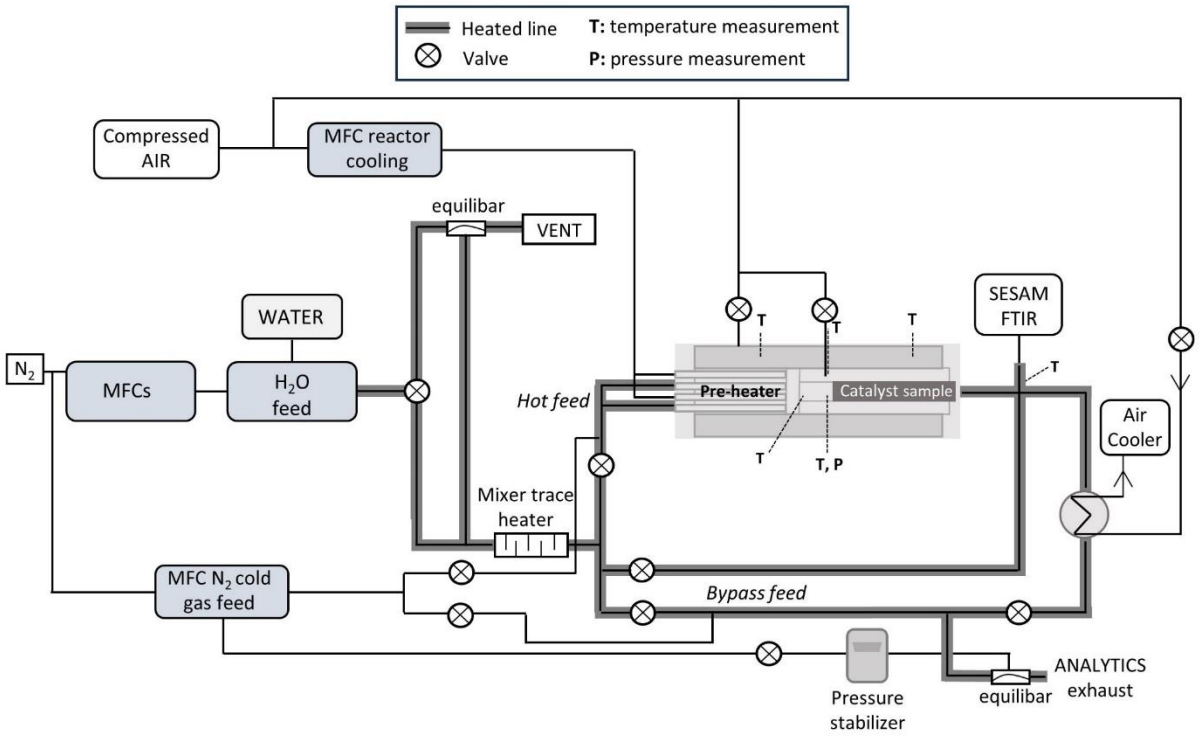

Figure 1: Synthetic Gas Bench (SGB) schematic configuration.

Three small-scale catalyst samples were tested: two diesel state-of the-art samples (a V-SCR and a Pt-AOC), and an ammonia engine tailored sample (an Fe-SCR). The characteristics of the samples are listed in Table 1. Both steady-state and light-off (temperature ramp) experiments are performed to derive kinetic information for the technologies of interest. These include NO_x reduction with NH_3, the effect of ANR on NO_x conversion, NH_3 slip and N_2O, the effect of N_2O addition in the feed gas as will be explained below.

Table 1: Properties of the tested catalyst samples.

Catalyst sample properties	**V-SCR**	**Fe-SCR**	**Pt-AOC**
Diameter x Length [mm x mm]	28 x 90	28 x 150	28 x90
CPSI [-]	100	230	200
Wall thickness [mils]	2	9	2
Substrate material [-]	metal	cordierite	metal
Cell shape [-]	triangle	square	triangle

For the purpose of marine applications, it is crucial to assess also sulfur tolerance, as SO_2 is a predictable byproduct of conventional pilot-fuel combustion, particularly when high-S fuel is used (e.g., HFO). V-SCR catalysts have demonstrated sulfur tolerance [17]; therefore, this study focuses on exclusively examining the impact of SO_2 on the Fe-SCR catalyst. Firstly, the catalyst is exposed to SO_2 until saturation. Thereafter, an SCR experiment is conducted without any further S-exposure. Finally, potential desulfation as function of temperature is examined.

2.2. Mathematical model

The present study is performed using the *ExothermiaSuite*® simulation tool [18]. The underlying models uses common assumptions to model the flow and thermophysical and chemical phenomena in the catalyst channels. These include the assumption of uniform flow, temperature, and concentration distribution at the inlet of the channels, and negligible heat losses to the ambient. Consequently, a one-dimensional (1D) representation of a single channel is adopted.

Temperature and species concentrations within the channel are determined by solving quasi-steady state balance equations for the heat (equation 1) and mass (equation 2) transfer:

$$\rho_{\mathrm{g}} C_{\mathrm{p,g}} v_{\mathrm{g}} \frac{\partial T_{\mathrm{g}}}{\partial z} = -h * \left(\frac{S_{\mathrm{F}}}{\varepsilon}\right) * \left(T_{\mathrm{g}} - T_{\mathrm{s}}\right) \tag{1}$$

$$\frac{\partial \left(v_{\mathrm{g}} y_{\mathrm{g},j}\right)}{\partial z} = -k_j * \left(\frac{S_{\mathrm{F}}}{\varepsilon}\right) * \left(y_{\mathrm{g},j} - y_{\mathrm{s},j}\right) \tag{2}$$

The wall surface temperature is calculated by the transient energy balance of the solid phase expressed as (equation 3):

$$\rho_{\mathrm{s}} C_{\mathrm{p,s}} \frac{\partial T_{\mathrm{s}}}{\partial t} = \lambda_{s,z} \frac{\partial^2 T_{\mathrm{s}}}{\partial z^2} + S \tag{3}$$

The surface concentrations are obtained by solving the concentration field inside the washcoat layer via the reaction-diffusion equation (equation 4):

$$-D_{w,j} \frac{\partial^2 y_{s,j}}{\partial w^2} = \sum_k n_{j,k} R_k \tag{4}$$

The solution of the concentration field in the washcoat layer is of particular importance for the case of technologies with multiple catalytic layers (1D + 1D). In fact, this is the case with ASCs that usually contain both a precious metal (PGM) layer, particularly an AOC layer of the oxidation of NH_3, as well as an SCR layer on top (Figure 2). This combination comes with advantages concerning NH_3 reduction and selectivity properties of the ASC, as NO_x formed in the oxidation layer diffuses through the SCR layer where it can be reduced.

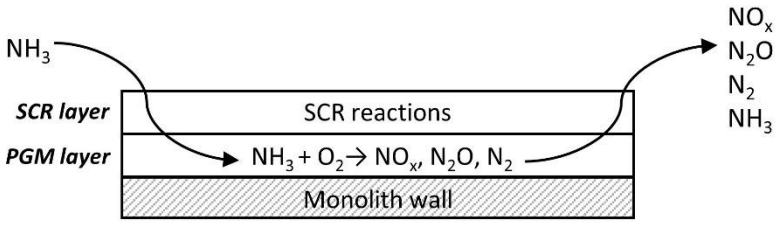

Figure 2: Dual-layer ASC schematic configuration.

2.3. Reaction Mechanisms

The SCR reactivity was described adapting commonly used SCR reaction schemes [19], including the standard, fast and NO_2 SCR reactions, as well as NH_3 and NO oxidation, and N_2O formation pathways as listed in Table 2. These reactions, commonly used in Diesel exhaust, are the starting point for developing the final models for the V- and Fe-SCR for the NH_3 engine exhaust.

Table 2; Basic SCR reaction scheme.

Reaction type	**Reaction**
NH_3 storage/release	$NH_3 \leftrightarrow NH_3$*
Standard SCR	$4\ NH_3$* + $4\ NO + O_2 \rightarrow 4\ N_2 + 6\ H_2O$
Fast SCR	$4\ NH_3$* + $2\ NO + 2\ NO_2 \rightarrow 4\ N_2 + 6\ H_2O$
NO_2 SCR	NH_3* + $3/4\ NO_2 \rightarrow 7/8\ N_2 + 3/2\ H_2O$
N_2O formation pathways	$2\ NH_3$* + $2\ NO + O_2 \rightarrow N_2 + N_2O + 3\ H_2O$ $4\ NH_3$* + $4\ NO_2 \rightarrow 2\ N_2 + 2\ N_2O + 6\ H_2O$
NO oxidation to NO_2	$NO + 1/2\ O_2 \leftrightarrow NO_2$
NH_3 oxidation	$4\ NH_3$* + $5\ O_2 \rightarrow 4\ NO + 5\ H_2O$ $2\ NH_3$* + $3/2\ O_2 \rightarrow N_2 + 3\ H_2O$ $4\ NH_3$* + $4\ O_2 \rightarrow 2\ N_2O + 6\ H_2O$

Ammonia oxidation on the Pt-AOC catalyst is approached with a simple kinetic model that gives a good representation of the overall reactions [20]. The common oxidation reactions used are listed in Table 3. These include the oxidation of NH_3 to N_2 and NO, the simultaneous oxidation of NH_3 and NO to N_2O and the oxidation of NO to NO_2.

Table 3: Basic Pt-AOC reaction scheme.

Reaction type	**Reaction**
NO oxidation to NO_2	$NO + 1/2\ O_2 \leftrightarrow NO_2$
NH_3 and NO oxidation to N_2O	$2\ NH_3 + 2\ NO + 3/2\ O_2 \rightarrow 2\ N_2O + 3\ H_2O$
NH_3 oxidation	$4\ NH_3 + 5\ O_2 \rightarrow 4\ NO + 5\ H_2O$ $2\ NH_3 + 3/2\ O_2 \rightarrow N_2 + 3\ H_2O$

3. Reaction model

3.1. V-SCR reaction model calibration

The results of the V-SCR activity tests are summarized in Figure 3 along with the respective calibrated model results. At temperatures above 300 °C, it is observed that the SCR process highly depends on the proportion of NO_x and NH_3 in the feed gas. When ANR is greater than 1, NO_x is almost fully converted, however this leads to increased NH_3 slip. When ANR is less than 1, partial NO_x conversion is achieved as expected from the SCR reaction stoichiometry (Table 2). Concerning N_2O, low selectivity (below 20 ppm) is observed in the temperature range below 500 °C. (Figure 3c). In order to examine the possible reduction of N_2O over the V-SCR catalyst, N_2O is added to the feed gas (Figure 3d). It is evident that N_2O flows through the catalyst unreacted at temperatures below 400 °C whereas N_2O is produced at 500 °C. The reaction rates of the reaction scheme listed in Table 2 are calibrated to fit the experimental determined NO_x, NH_3 and N_2O keeping the same values for the entire range of test conditions.

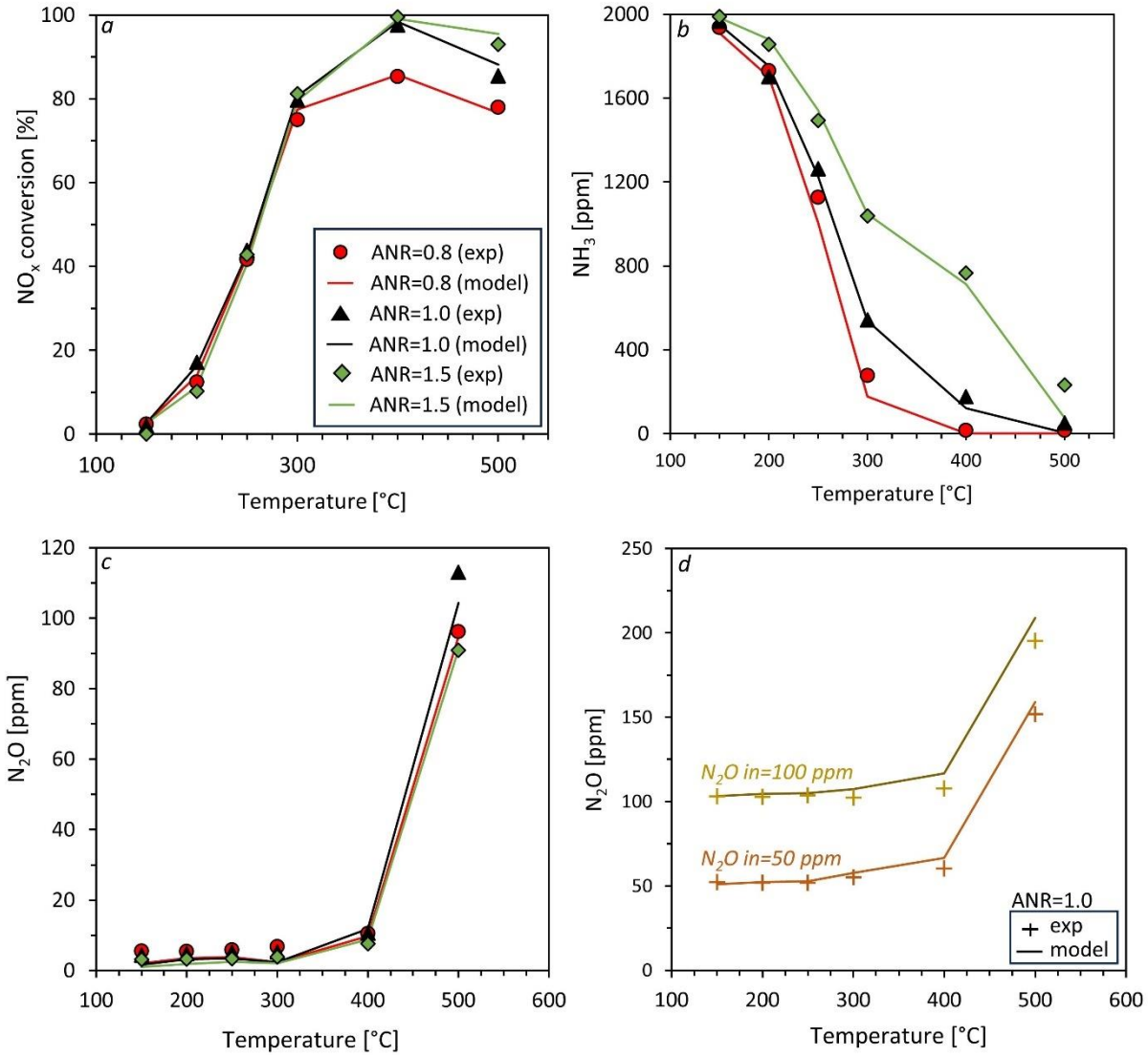

Figure 3: (a) NO_x conversion, (b) NH_3 slip, (c) N_2O without N_2O in the feed gas, under various NH_3/NO_x ratios, and (d) N_2O with 50 ppm and 100 ppm N_2O in the feed gas under ANR=1.0, over the V-SCR, based on the experimental data (symbols) and the model (solid lines) (Feed gas: 2000 ppm NO, ANR=0.8, 1.0, 1.5, 10% O_2, 15% H_2O, N_2 balance, GHSV=20,000 $^{h-1}$).

3.2. Fe-SCR reaction model calibration

For the development of the reaction kinetic model of the Fe-SCR catalyst, several modifications of the commonly used reactions in SCR technologies (Table 2) were required. Figure 4 a shows NO_x and NH_3 conversion under SCR conditions According to the standard SCR reaction (4 NO + 4 NH_3 + O_2 → 4 N_2 + 6 H_2O) equal number of moles of NO_x and NH_3 are expected to react. However, test results revealed an overconsumption of NH_3 compared to NO_x. This is also evident in Figure 4b, where $\Delta NH_3/\Delta NO_x$ is greater than 1 in the whole temperature range. This phenomenon has been documented in several previous studies [21-24]. Consequently, for the model development the stoichiometry of the typical standard SCR reaction was modified as below:

$$6\ NH_3{}^* + 5\ NO + 2\ O_2 \rightarrow 11/2\ N_2 + 9\ H_2O \qquad (5)$$

The modified standard SCR reaction is able to successfully predict the overconsumption of NH_3 (solid lines of Figure 4).

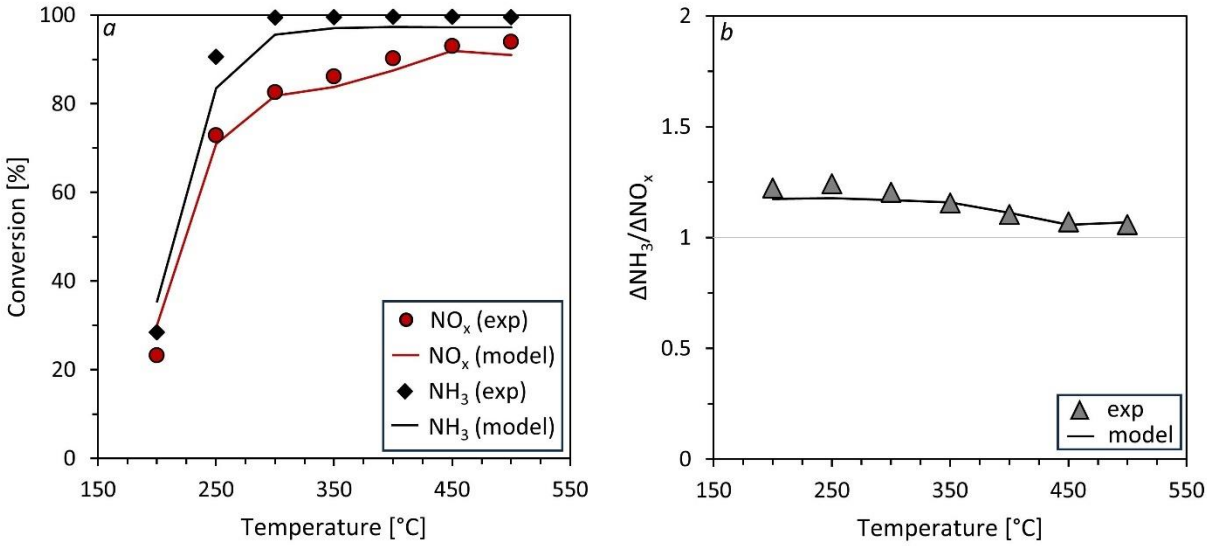

Figure 4: (a) NO_x and NH_3 conversion under Standard SCR conditions, and (b) $\Delta NH_3/\Delta NO_x$ over the Fe-SCR, based on the experimental data (symbols) and the model (solid lines) (Feed gas: 1000 ppm NO, ANR=1.0, 10% O_2, 15% H_2O, N_2 balance, GHSV=14,000 $^{h-1}$).

The experimental findings on the influence of the inlet ANR are depicted in Figure 5a with symbols. When ANR is less than 1, the catalyst performance is limited by the lack of NH_3 to further react with NO_x. When abundant NH_3 is present (ANR>1), NO_x conversion increases at temperatures above 350 °C. At temperatures below 300 °C and in excess of NH_3, NO_x conversion is significantly reduced. To capture this phenomenon in the model, it was necessary to include an inhibition term (1 + k x C_{NH3}^2) in the reaction rate of the modified standard SCR (reaction 5):

$$R = k \cdot \Psi_S \cdot \psi_{S_{NH_3}} \cdot C_{NO} \cdot C_{O_2} / (1+k \cdot C_{NH_3}{}^2) \quad (6)$$

The introduction and calibration of the inhibition term results in a good accuracy between the model and the experiment (solid lines of Figure 5a). The conversion of NO_x with and without the inhibition term for the case of ANR=3.0, is shown in Figure 5b.

Excess NH_3 leads to increased concentrations of NH_3 slip, while in the case of stoichiometric ANR or deficiency of NH_3, NH_3 completely reacts with NO_x (Figure 5c). Selectivity of N_2O is maintained at low levels (<10 ppm) and it is not affected by NH_3/NO_x ratio (Figure 5d).

In order to explain the NO_x emissions as function of temperature (Figure 6a), it was necessary to add an SCR reaction with N_2O acting as a 'promoting' species. This is realized by adding N_2O in both the reactants and products (standard SCR + N_2O):

$$NH_3{}^* + NO + ¼\ O_2 + N_2O \rightarrow N_2 + 3/2\ H_2O + N_2O \quad (7)$$

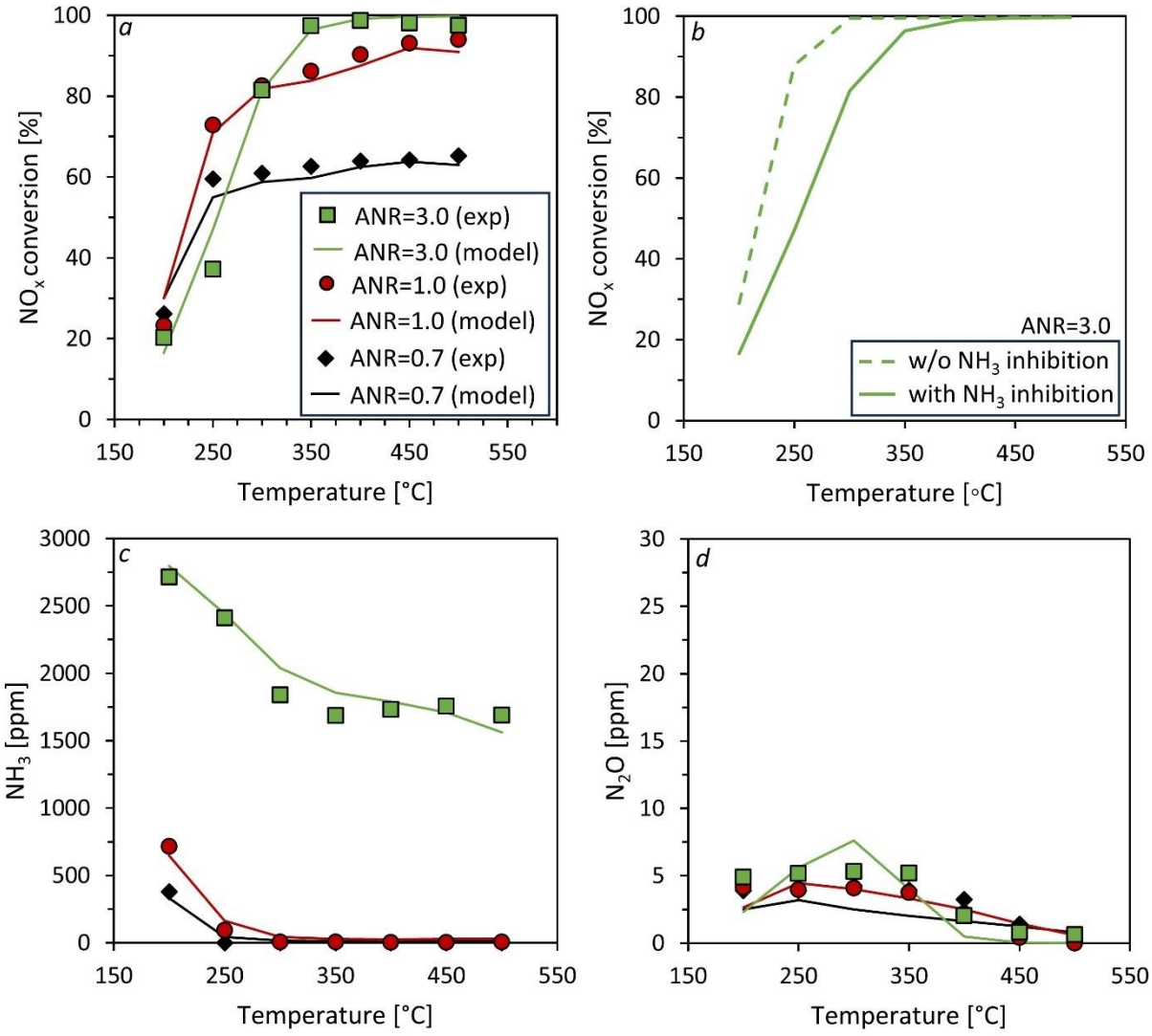

Figure 5: (a) Comparison of the experimental data and the model of (a) NO_x conversion under various ANR including the inhibition term, (b) under ANR=3.0 with and without the inhibition term, (c) NH_3 slip under various ANR ratios, and (d) N_2O selectivity under various ANR ratios, over the Fe-SCR (Feed gas: 1000 ppm NO, ANR=0.7, 1.0, 3.0, 10% O_2, 15% H_2O, N_2 balance, GHSV=14,000 $^{h-1}$).

This way, the reaction is activated only in the presence of N_2O with no effect on the N_2O concentration in the exhaust gas. The addition of this reaction resulted in very good accuracy of the model both in the presence and absence of N_2O (solid lines of Figure 6a). Figure 6b shows that in the presence of N_2O, reaction 7 is dominant while the reaction rate of the modified standard SCR (reaction 5) decreases due to competition between the two reactions.

Finally, N_2O conversion under various NH_3 concentrations is examined (Figure 7). As ANR increases, N_2O conversion also increases reaching a maximum at ANR=1.4. Further increase of NH_3 in the feed gas has a negative effect on N_2O reduction, especially at the lower temperatures (350 °C and 400 °C). To model N_2O conversion, the global reaction of direct reduction of N_2O by NH_3 (reaction 8) [25, 26] together with the global reaction of the simultaneous reduction of NO and N_2O by NH_3 (reaction 9) [27] are added to the reaction scheme:

$$2\ NH_3{}^* + 3\ N_2O \rightarrow 4\ N_2 + 3\ H_2O \qquad (8)$$

$$2\ NH_3{}^* + 2\ NO + N_2O \rightarrow 3\ N_2 + 3\ H_2O \quad (9)$$

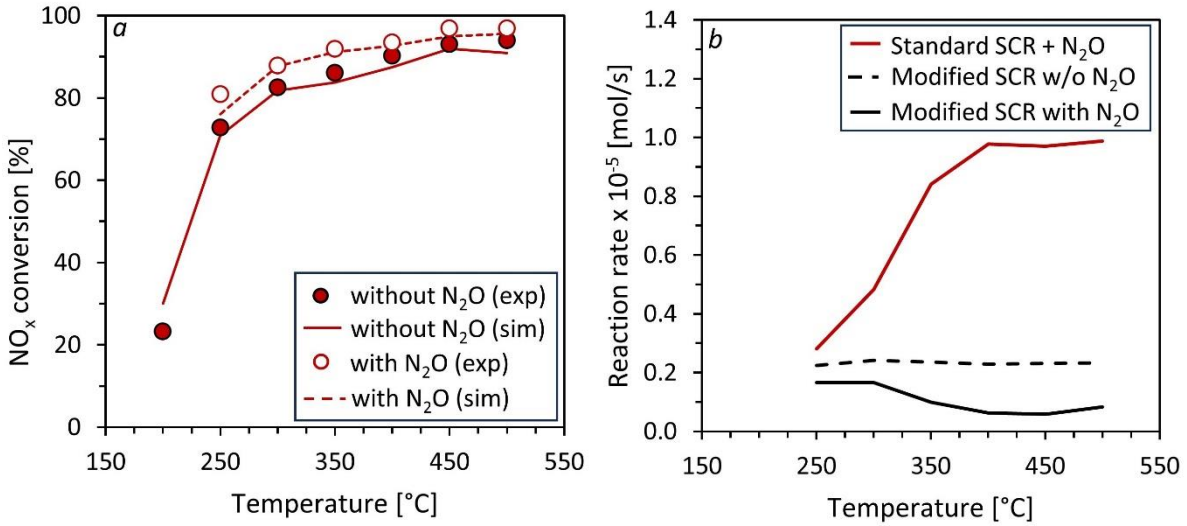

Figure 6: (a) NO_x conversion with and without N_2O and (b) reaction rates of the Standard SCR + N_2O and the modified stoichiometry SCR in the presence and absence of N_2O, over the Fe-SCR, based on the experimental data (symbols) and the model (solid lines) (Feed gas: 1000 ppm NO, ANR=1.0, 0 and 100 ppm N_2O, 10% O_2, 15% H_2O, N_2 balance, GHSV=14,000 $^{h-1}$).

For the efficient modeling of N_2O conversion in the whole range of ANR it was necessary to include an NH_3 inhibition term ($1 + k \times C_{NH3}{}^{1.5}$) to the reaction rate of the direct reduction of N_2O by NH_3 (reaction 8) as:

$$R_r = k \cdot \Psi_S \cdot \psi_{S_{NH_3}} \cdot C_{N2O} / (1+k \cdot C_{NH_3}{}^{1.5}) \quad (10)$$

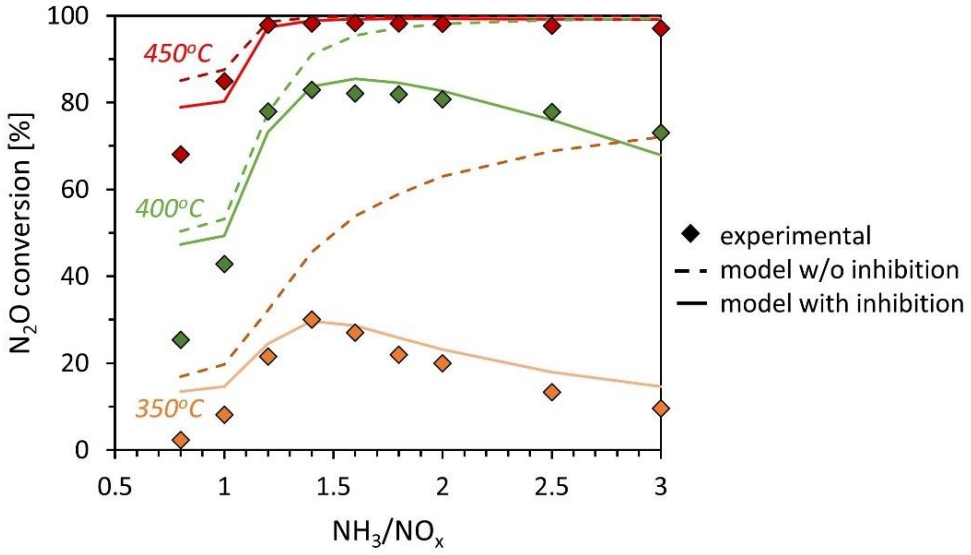

Figure 7: N_2O conversion under various NH_3/NO_x ratios, based on the experimental data (symbols) and the model without (dashed line) and with (solid line) the inhibition term, over the Fe-SCR. (Feed gas: 1000 ppm NO, variable NH_3, 100 ppm N_2O, 10% O_2, 15% H_2O, N_2 balance, GHSV=14,000 $^{h-1}$).

Considering all the necessary modifications, the final Fe-SCR reaction scheme adopted is summarized in Table 1Table 4.

Table 4: Fe-SCR reaction scheme.

Reaction type	**Reaction**
NH_3 storage/release	$NH_3 \leftrightarrow NH_3$*
Modified Standard SCR Standard SCR (+N_2O)	6 NH_3* + 5 NO + 2 O_2 → 11/2 N_2 + 9 H_2O NH_3* + NO + 1/4 O_2 + N_2O → N_2 + 3/2 H_2O +N_2O
Fast SCR	NH_3* + ½ NO + ½ NO_2 → N_2 + 3/2 H_2O
N_2O formation pathways	2 NH_3* + 2 NO + O_2 → N_2 + N_2O + 3 H_2O 2 NH_3* + 2 NO_2 → N_2 + N_2O + 3 H_2O
NO oxidation to NO_2	NO + 1/2 O_2 ↔ NO_2
NH_3 oxidation to N_2	NH_3* + 3/4 O_2 → ½ N_2 + 3/2 H_2O
N_2O reduction by NH_3	2 NH_3* + 3 N_2O → 4 N_2 + 3 H_2O
Simultaneous reduction of NO and N_2O by NH_3	2 NH_3* + 2 NO + N_2O → 3 N_2 + 3 H_2O

3.3. Pt-AOC reaction model calibration

The experimental results compared to the simulation model of the Pt-AOC catalyst are presented in Figure 8. Here the focus is not only on NH_3 reduction, but also on the formation of the unwanted NO_x and N_2O. The concentration of NH_3 decreases sharply from 200 °C to 250 °C and is completely oxidized around 300 °C. Production of N_2O is observed above 200 °C and increases significantly up to a maximum of 100 ppm at 250 °C. Above that temperature, formation of NO ad NO_2 are favored while N_2O is simultaneously decreasing. It is worth noting that the calibrated model using the common reactions of Table 3, is capable of capturing the complex trends with respect to N_2O and NO_x byproducts in the whole temperature range.

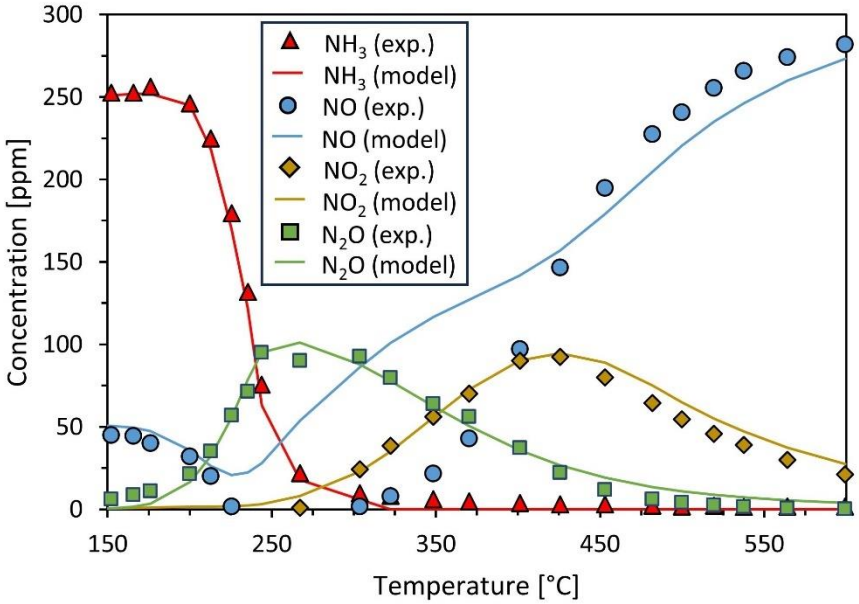

Figure 8: Comparison of the NH_3, NO, NO_2 and N_2O outlet concentrations for NH_3 oxidation over the Pt-AOC based on the experimental data (symbols) and the model (solid lines) (Feed gas: 250 ppm NH_3, 50 ppm NO, 6% O_2, 15% H_2O, 15 ppm SO_2, N_2 balance, GHSV=20,000 $^{h-1}$).

4. Sulfur saturation of the Fe-SCR

The Fe-SCR was initially exposed to 110 ppm SO_2 at 225 °C until saturation (approximately 25 minutes) as presented in Figure 9a. The maximum SO_2 stored on the catalytic sites is calculated equal to 1.13 g/l. Thereafter, an SCR experiment is conducted without any further S-exposure (Figure 9b). Compared to the fresh catalyst, reduced NO_x conversion is observed at temperatures below 300 °C. At higher temperatures, NO_x conversion efficiency was not affected by S-saturation. Concerning N_2O, the saturated catalyst shows similar activity to the fresh (Figure 9c). The desulfation at high temperatures is examined as depicted in Figure 9d. The catalyst is initially exposed at a high temperature (above 400 °C) for 30 minutes and then NO_x conversion is measured at 250 °C where NO_x conversion reduction was observed. At a desulfation temperature of 450 °C the catalyst efficiency is partially retrieved while the catalyst activity is fully recovered at 600 °C.

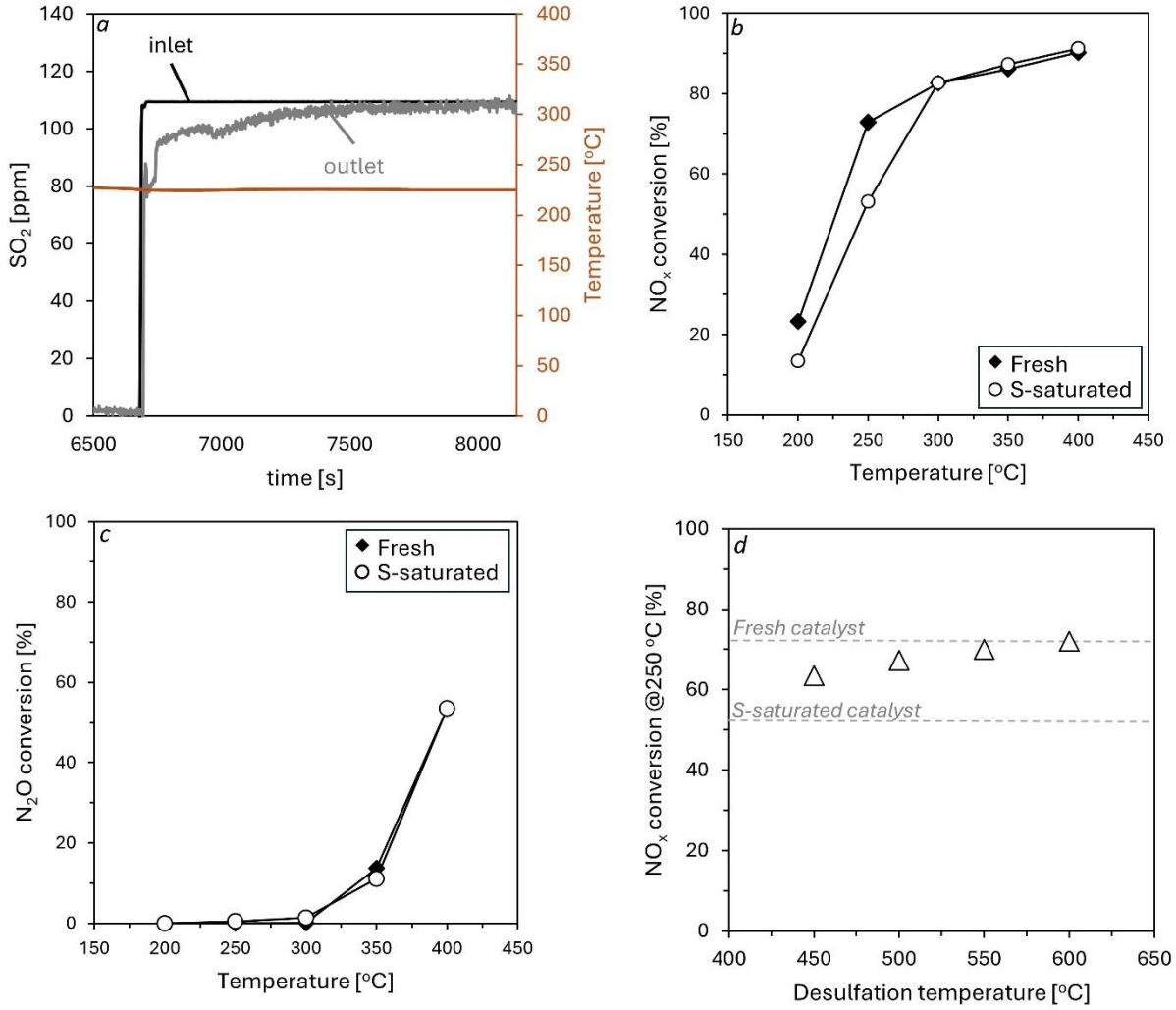

Figure 9: (a) Exposure of the Fe-BEA catalyst to SO_2, (b) NOx conversion of the fresh and s-saturated catalyst, (c) N_2O conversion of the fresh and s-saturated catalyst, (d) Desulfation of the catalyst at high temperatures (Feed gas (a): 110 ppm SO_2, 1000 ppm NO, ANR=1.0, 15% H_2O, 10% O_2, N_2 balance, GHSV=14,000 h^{-1}; Feed gas (b), (c), (d): 1000 ppm NO, ANR=1.0, 100 ppm N_2O, 15% H_2O, 10% O_2, N_2 balance, GHSV=14,000 h^{-1}).

5. Model Application in Marine Engine Exhaust

The objective of this section is to illustrate the application of modeling in the design phase of the NH_3 marine engine EATS. Given that NH_3 engines are still under development and yet commercially available, precise data on their exhaust gas conditions and emission concentrations remain unavailable. Consequently, the exhaust gas conditions of low-speed marine diesel engines are used as a basis, assuming a high-pressure (pre-turbo) EATS [28,29].

Ammonia combustion is likely to produce high levels of unburnt NH_3. It is well known that the molar ratio of NH_3/NO_x in the exhaust gas is very critical for the operation of the SCR. Recent studies [30,31] show that N_2O formation occurs in locations with significant unburnt NH_3 which is eliminated when unburnt NH_3 decreases and NO_x emissions increase. Based on these trends, two scenarios are examined: (1) high NO_x emissions with low NH_3 and N_2O (ANR<1), and (2) high unburnt NH_3 and N_2O with low NO_x emissions (ANR>1).

The simulated inlet conditions of the EATS are detailed in Table 5.

Table 5: Assumed inlet conditions of the EATS.

Engine Load [%]	**25**	**50**	**75**	**100**
Exhaust gas temperature [°C]	290	310	350	410
Exhaust gas pressure [bar]	1.4	2.1	3.1	4.0
Exhaust gas mass flow rate [kg/s]	4	9	12	15
Exhaust gas composition for ANR<1 and low N_2O	1000 ppm NO, 500 ppm NH_3, 30 ppm N_2O, 10% H_2O, 10% O_2, N_2 balance			
Exhaust gas composition for ANR>1 and high N_2O	1000 ppm NO, 3000 ppm NH_3, 100 ppm N_2O, 10% H_2O, 10% O_2, N_2 balance			

In the case of NH_3 shortage and low N_2O (ANR<1), NH_3 injection upstream of the SCR is required as shown in Figure 10a to achieve the regulated NO_x limit of 3.4 g/kWh. In the case of excessive NH_3, a dual-layer ASC is placed downstream of the SCR to treat the unreacted NH_3 of the deNO_x process (Figure 10b). The ASC is assumed to be a combination of an SCR layer and a precious metal-based layer (AOC). The composition of the SCR layer is identical to the SCR catalyst prior the ASC. In both scenarios the commonly used V-SCR is compared to Fe-SCR.

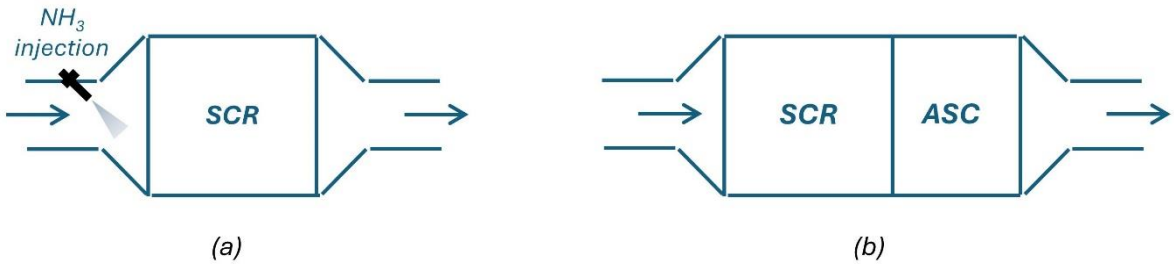

Figure 10: Model exhaust layouts for the two cases examined: (a) shortage of NH_3 with low N_2O, and (b) excess of NH_3 with high N_2O in the exhaust gas.

Besides NO_x and NH_3 control, CO_2 equivalent emissions are calculated at the system outlet, accounting for both N_2O (originating from NH_3 combustion and the EATS), and CO_2 from pilot-fuel combustion (CO_2-equivalent = N_2O x 300 + CO_2 from pilot fuel). For the latter, 5% Diesel pilot-fuel is assumed.

Based on the assumed marine engine exhaust gas conditions presented in Table 5 and the weighting factors of the legislated E3 test cycle [32], it is estimated that a NO_x conversion rate in the order of 75% is required to comply with the Tier III limit of 3.4 gNO_x/kWh.

In the scenario of NH_3 shortage (ANR<1) and low N_2O emissions, where only the SCR is utilized, the minimum deNO_x requirement is met when NH_3 is injected at a target ANR of around 0.75. The volume of each technology is chosen in order to meet both NO_x and NH_3 limits, the latter set at 10 ppm. For the V-SCR the volume is equal to 1000 liters. When the Fe-SCR is used, the volume is increased to 1400 liters.

Applying the simulation model to the four loads of the E3 test cycle under the conditions specified in Table 5, NH_3 slip, N_2O and CO_2-equivalent emissions are calculated at the system outlet as depicted in Figure 11. For the V-SCR, nearly all NH_3 is predicted to be consumed during NO_x reduction,

resulting in NH_3 slip of less than 5 ppm, with minimal N_2O formation. When the V-SCR is replaced by the Fe-SCR catalyst, NH_3 slip is reduced to the limit of 10 ppm. Notably, N_2O emissions significantly reduce at 75% and 100% engine load, benefiting from the catalyst's ability to reduce both NO_x and N_2O. Consequently, the CO_2-equivalent emissions of the Fe-SCR are lower compared to those of the V-SCR catalyst. This scenario proposes a significant reduction of GHG emissions compared to Diesel-only operation of 70% that can even reach 90% at full load when the Fe-SCR is implemented.

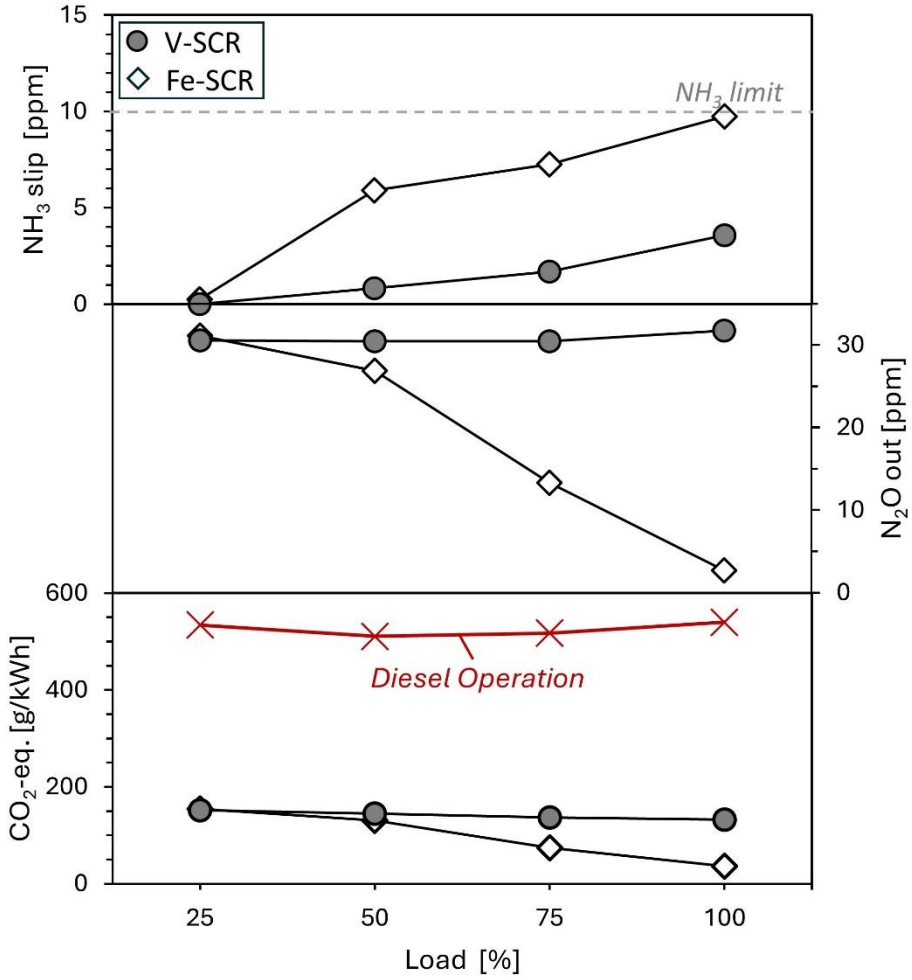

Figure 11: Model predictions for NH_3 slip, N_2O and CO_2-equivalent emissions over 100-year GWP at the SCR system outlet in the case of lack of NH_3 (ANR<1) and low N_2O in the exhaust gases. (Exhaust gas composition: 1000 ppm NO, 500 ppm NH_3, 30 ppm N_2O, 10% H_2O, 10% O_2, N_2 balance).

Figure 12 presents NO_x, NH_3, N_2O and CO_2-equivalent emissions for the case of excessive engine-out NH_3 (ANR>1) and high N_2O emissions.

For excessive NH_3 (ANR>1) and high N_2O emissions, the volume of the SCR catalysts in both technologies is assumed to be equal to 1000 liters. The volumes of the ASC catalysts are iteratively determined to reduce NH_3 below 10 ppm. For the V-SCR + ASC system, the ASC volume is 845 liters while for the Fe-SCR + ASC the respective volume is 700 liters. In this case, NO_x, NH_3, N_2O and CO_2-equivalent emissions are depicted in Figure 12. Increased ANR values lead to unreacted NH_3 at the SCR outlet, which is efficiently oxidized in the ASC (below 10 ppm). However, this oxidation process in the ASC promotes the formation of NO_x and N_2O. In the case of the Fe-SCR the N_2O emissions are significantly decreased compared to the V-SCR, especially at higher loads due to the deN_2O

capability of Fe-based catalysts. However, N_2O levels in both cases remain extremely high leading to unacceptable CO_2-equivalent emissions.

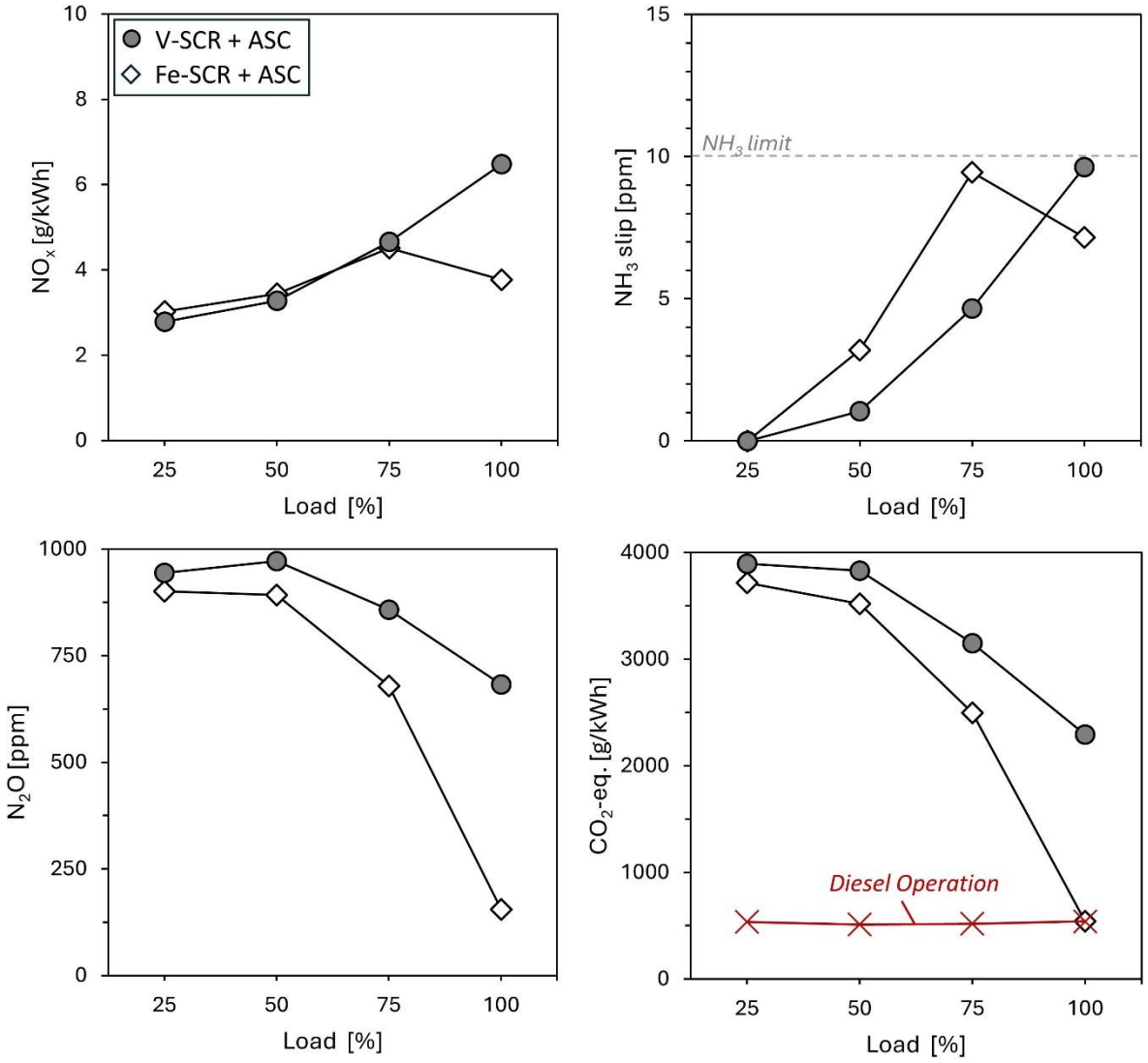

Figure 12: Model predictions for NO_x, NH_3 slip, N_2O and CO_2-equivalent emissions over 100-year GWP at the system outlet in the case of excessive NH_3 in the exhaust gases (ANR>1) (Feed gas: 1000 ppm NO, 3000 ppm NH_3, 100 ppm N_2O, 10% H_2O, 10% O_2, N_2 balance).

6. Preliminary results with Co-based deN_2O catalyst

Following the preliminary target to reduce N_2O emissions from ammonia combustion, N_2O decomposition of a cobalt-based catalyst is currently being tested and evaluated on the SGB. The preliminary experimental results are depicted in Figure 13. A first indication is that high N_2O conversion is achieved at elevated temperatures, however the effect of NO and NH_3 are yet to be determined to conclude the catalyst activity.

Thereafter, a model will be developed to be adapted in the EATS of ammonia-fueled engines.

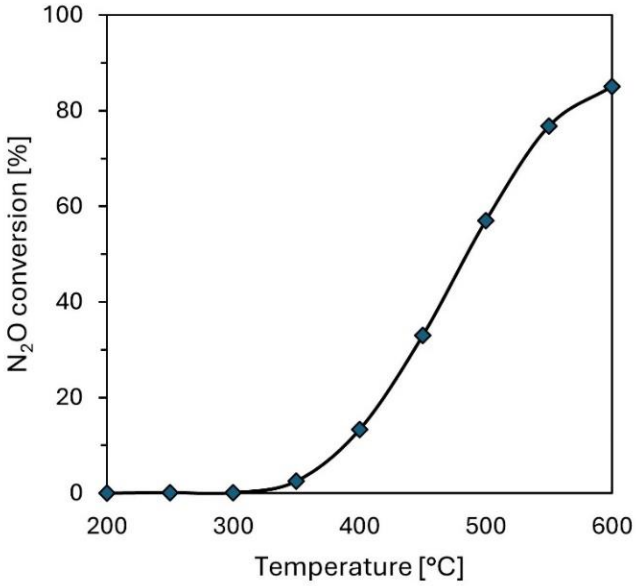

Figure 13: N_2O conversion (experimental) over the cobalt-based catalyst (Feed gas: 100 ppm N_2O, 10% H_2O, 10% O_2, 10 ppm SO_2, N_2 balance, GHSV=20,000 h^{-1}).

7. Conclusions & Future work

The main findings of the combined testing and modeling work presented here are summarized below:

- The performance of the V-SCR and the Pt-AOC catalysts are well predicted with commonly used literature reaction schemes.
- In the case of the Fe-SCR, special modifications of the chemical reaction scheme are necessary to accurately describe the occurring processes. These include the modification of the standard SCR reaction stoichiometry, inhibition of the modified standard SCR reaction by NH_3 at high NH_3 inlet concentrations and low temperatures, addition of the typical standard SCR with N_2O in both the reactants and products, and the inhibition of the direct N_2O reduction by NH_3 at high inlet concentrations of NH_3.
- Fe-SCR catalyst material was found to be sulfur tolerant in the operating range of large two-stroke marine engines.

The simulation study of the marine engine aftertreatment applications provided the following results:

- For low NH_3 and N_2O levels in the exhaust gas (ANR<1), NO_x conversion is optimized to comply with Tier III limits by NH_3 injection upstream of the SCR, resulting in low NH_3 slip levels. In addition, there is a significant reduction in CO_2-equivalent emissions by 70% to 90% (depending on the SCR technology) compared to diesel-only operation.
- For abundant NH_3 and high N_2O in the exhaust gas (ANR>1), unreacted NH_3 of the deNO_x process can be efficiently managed with an ASC. However, NH_3 oxidation promotes the formation of very high N_2O emissions, causing CO_2-equivalent emissions to reach up to 7 times the levels of diesel-only operation, rendering this configuration impractical.

Based on the above, an appropriate control strategy and optimization of the exhaust aftertreatment system, together with engine tuning of NH_3 combustion is essential to tackle both noxious and GHG

emissions. As the ultimate goal is complete decarbonization of the maritime sector, the future steps include:

- Further experimental investigation on the performance of the deN_2O cobalt-based catalyst followed by model development using the test data.
- Application of the new catalyst models in the exhaust gas stream of NH_3 engines.
- Development and optimization of the complete exhaust aftertreatment system and controls for NH_3 marine engine applications.

Funding

This work has been funded by the ENGIMMONIA project, which has received funding from the European Union's Horizon 2020 research and innovation program under grant agreement Nr. 955413.

Acknowledgments

The authors would like to acknowledge support of this work by Ecospray for providing the V-based and Pt-based catalyst samples and TOPSOE for providing the Fe-based catalyst sample and useful discussions during the experimental campaign.

Nomenclature

A. Latin letters

C_P	Specific heat capacity *J/(kg·K)*
D_w	Effective diffusivity m^2/s
h	Heat transfer coefficient *W/(m²·K)*
k_j	Mass transfer coefficient *m/s*
n	Stoichiometric coefficient -
R_k	Reaction rate *mol/(m³·s)*
S	Heat source term W/m^3
S_F	Monolith specific surface area m^2/m^3
T	Temperature *K*
v	Velocity *m/s*
w	Dimension perpendicular to wall surface -
y_j	Molar fraction -
z	Axial coordinate along monolith *m*

B. Greek letters

ε	Macroscopic void fraction -
λ	Thermal conductivity *W/(m·K)*
ρ	Density kg/m^3

C. Subscripts and Superscripts

g	Exhaust gas
j	Species index
k	Reaction index
s	Solid

Literature

[1] International Maritime Organization. Fourth IMO GHG Study Full Report; International Maritime Organization: London, UK, 2020.

[2] Liu, L.; Wu, J.; Liu, H.; Wu, Y.; Wang, Y. Investigation of combustion and emission characteristics in a low-speed marine engine using ammonia under thermal and reactive atmospheres. *Int. J. Hydrogen Energy* **2024**, 1237-1247.

[3] IMO Marine Environment Protection Committee. Eightieth Session (MEPC 80)-Summary Report; International Maritime Organization: London, UK, 2023.

[4] Ni, P.; Wang, X.; Li, H. A review on regulations, current status, effects and reduction strategies of emissions for marine diesel engines. *Fuel* **2020**, 279, 118477.

[5] Xu, L.; Xu, S.; Bai, X. S.; Repo, J. A.; Hautala, S.; Hyvönen, J. Performance and Emission Characteristics of an Ammonia/Diesel Dual-Fuel marine engine. *Renewable and Sustainable Energy Reviews* **2023**, 185, 113631.

[6] DNV GL AS Maritime. Comparison of Alternative Marine Fuels Report, SEA/LNG Ltd, Norway 2019.

[7] Rodríguez, C.G.; Lamas, M.I.; Rodríguez, J.d.D.; Abbas, A. Possibilities of Ammonia as Both Fuel and NOx Reductant in Marine Engines: A Numerical Study. *J. Mar. Sci. Eng.* **2022**, 10, 43.

[8] Wang, Q.; Yang, W.; Dang, H.; Li, L.; Wu, R.; Wang, Y.; Zhao, Y. Enhancement of N_2O Decomposition Performance by co-doping of Ni and Y to Co_3O_4 catalyst. *J. Environmental Chemical Engineering* **2024**, 12, 112463.

[9] Nova, I.; Tronconi, E. Fundamental and Applied Catalysis Urea-SCR Technology for deNO_x after Treatment of Diesel Exhausts; Springer: Berlin/Heidelberg, Germany, 2014.

[10] Han, J.; Wang, A.; Isapour, G.; Härelind, H.; Skoglundh, M.; Creaser, D.; Olsson, L. N_2O Formation during NH_3-SCR over Different Zeolite Frameworks: Effect of Framework Structure, Copper Species, and Water. *Ind. Eng. Chem. Res.* **2021**, 60, 17826–17839.

[11] Wang, A.; Wang, Y.; Walter, E.D.; Kukkudapu, R.K.; Guo, Y.; Lu, G.; Weber, R.S.; Wang, Y.; Peden, C.H.F.; Gao, F. Catalytic N_2O decomposition and reduction by NH_3 over Fe/Beta and Fe/SSZ-13 catalysts. *J. Catal.* **2018**, 358, 199–210.

[12] Zabilskiy, E. In-situ XAS Study of Catalytic N_2O Decomposition over CuO/CeO_2 Catalysts. *ChemCatChem* **2021**, 13, 1814–1823.

[13] Komvokis, V.G.; Marnellos, G.E.; Vasalos, I.A.; Triantafyllidis, K.S. Effect of Pretreatment and Regeneration Conditions of Ru/γ-Al_2O_3 Catalysts for N_2O Decomposition and/or Reduction in O_2 -rich Atmospheres and in the Presence of NO_x, SO_2 and H_2O. *Appl. Catal. B Environ.* **2009**, 89, 627–634.

[14] Hermes, A.C.; Hamilton, S.M.; Hopkins, W.S.; Harding, D.J.; Kerpal, C.; Meijer, G.; Fielicke, A.; Mackenzie, S.R. Effects of Coadsorbed Oxygen on the Infrared Driven Decomposition of N_2O on Isolated Rh^{5+} Clusters. *J. Phys. Chem. Lett.* **2011**, 2, 3053–3057

[15] Xie, P.; Luo, Y.; Ma, Z.; Wang, L.; Huang, C.; Yue, Y.; Hua, W.; Gao, Z. CoZSM-11 Catalysts for N_2O Decomposition: Effect of Preparation Methods and Nature of Active Sites. *Appl. Catal. B Environ.* **2015**, 170, 34–42.

[16] Farhan, K.M.; Thabassum, A.; Ismail, T.M.; Sajith, P.K. Theoretical Investigation into the Effect of Water on the N_2O Decomposition Reaction over the Cu-ZSM-5 Catalyst. *Catal. Sci. Technol.* **2022**, 12, 1466–1475.

[17] Busca, G.; Lietti, L.; Ramis, G.; Berti, F.; Chemical and mechanistic aspects of the selective catalytic reduction of NOx by ammonia over oxide catalysts: A review. *Applied Catalysis B: Environmental 18* **1998**, 1-36.

[18] Exothermia, S.A. Exothermia Suite User Manual, version 2022.3; Gamma Technologies, LLC: Westmont, IL, USA, 2022.

[19] Karamitros, D.; Koltsakis, G. Model-based optimization of catalyst zoning on SCR-coated particulate filters. *Chem. Eng. Sci.* **2017**, 173, 514-524.

[20] Colomb, M.; Nova, I.; Tronconi, E.; Schmeißer, V.; Brandl-Konrad, B.; Zimmermann, L.R. Experimental Modeling Study of a dual-layer (SCR + PGM) NH_3 slip monolith catalyst (ASC) for automotive SCR aftertreatment systems. Part I. Kinetics for the PGM Component and Analysis of SCR/PGM Interactions. *Appl. Catal. B Environ*. **2013**, 142–143, 861–876.

[21] Sjövall, H.; Blint, R. J.; Gopinath, A.; Olsson, L. A Kinetic Model for the Selective Catalytic Reduction of NO_x and NH_3 over an Fe-zeolite Catalyst. *Ind. Eng. Chem. Res.* **2010**, 49, 39-52.

[22] Nedyalkova, R.; Kamasamudram, K.; Currier, N. W.; Li, J.; Yezerets, A. Experimental evidence of the mechanism behind NH_3 overconsumption during SCR over Fe-zeolites. *Journal of Catalysis* **2013**, 299, 101-108.

[23] Bacher, V.; Perbandt, C.; Schwefer, M.; Siefert, R.; Pinnow, D.; Turek, T. Kinetics of ammonia consumption during the selective catalytic reduction of NO_x over an iron zeolite catalyst. *Applied Catalysis B: Environmental* **2015**, 162, 158-166.

[24] Liu, Q.; Bian, C.; Ming, S.; Guo, L.; Zhang, S.; Pang, L.; Liu, P.; Chen, Z.; Li, T. The opportunities and challenges of iron-zeolite as NH_3-SCR catalyst in purification of vehicle exhaust. *Applied Catalysis A* **2020** ,607, 117865.

[25] Aika, K.; Oshihara, K. Nitrous oxide reduction with ammonia over Co-MgO catalyst and the influence of excess oxygen. *Catalysis Today* **1996**, 29, 123-126.

[26] Zhang, X.; Shen, Q.; He, C.; Ma, C.; Chen, J.; Li, L.; Hao, Z. Investigation of Selective Catalytic Reduction of N_2O by NH_3 over an Fe-Mordenite Catalyst: Mechanism and O_2 Effect. *ASC Catal.* **2012**, 2, 512-520.

[27] Coq, B.; Mauvezin, M.; Delahay, G.; Butet, J. B.; Kieger, Stephane. The simultaneous catalytic reduction of NO and N_2O by NH_3 using an Fe-zeolte-beta catalyst. *Applied Catalysis B: Environmental* **2000**, 27, 193-198.

[28] Zhu, Y.; Xia, C.; Shreka, M.; Wang, Z.; Yuan, L.; Zhou, S.; Feng, Y.; Hou, Q.; Ahmed, S.A. Combustion and emission characteristics for a marine low-speed diesel engine with high-pressure SCR system. *Environ. Sci. Pollut. Res*. **2020**, 27, 12851–12865.

[29] Zhu, Y.; Li, T.; Xia, C.; Feng, Y.; Zhou, S. Simulation analysis on vaporizer/mixer performance of the high-pressure SCR system in a marine diesel. *Chem. Eng. Process.-Process Intensif.* **2020**, 148, 107819.

[30] Northrop, W. F. Modeling nitrogen species from ammonia reciprocating engine combustion in temperature-equivalence ratio space. *Applications in Energy and Combustion Science 17* **2024**, 100245.

[31] Reggeti, S. A.; Northrop, W. F. Lean ammonia-fueled engine operation enabled by hydrogen-assisted turbulent jet ignition. *Front. Mech. Eng.* **2024**, 10:1368717.

[32] MARPOL, Annex VI—Regulations for the Prevention of Air Pollution from Ships, Appendix II—Test Cycles and Weighting Factors (Regulation 13). Available online: http://www.marpoltraining.com/MMSKOREAN/MARPOL/Annex_VI/app2.htm